EurJIC European Journal of Inorganic Chemistry

ChemPubSoc Europe

FULL PAPER

DOI:10.1002/ejic.201500629

Doped Framework Iron Hydroxyl Phosphate as Photocatalyst for Hydrogen Production from Water/Methanol Mixtures

Marco Serra,[a] Herme G. Baldovi,[a] Mercedes Alvaro,[a] and Hermenegildo Garcia*[a]

Keywords: Photocatalysis / Semiconductors / Doping / Hydrogen / Iron

In the search for novel photocatalysts for hydrogen production and with the α-Fe_2O_3 photoelectrocatalyst as a recent precedent, we report herein the preparation, semiconductor properties and photocatalytic activity of metal-doped (0.1–5 wt.-% loading) iron hydroxyl phosphate (FeP). X-ray diffraction analyses of FeP samples subjected to extended photocatalytic irradiation showed the stability of this framework phosphate under photocatalytic conditions. Doping increased the photocatalytic efficiency of FeP for all dopants, with the optimal doping level between 0.1 and 1 %. Under the optimized conditions (Cr at 1 % doping), the photocatalytic activity of FeP reached a hydrogen production rate of 35.82 μmol g_{Fe}^{-1} in the absence of platinum as co-catalyst. The conduction flat band potential was estimated by photocurrent measurements or impedance spectroscopy to be 0.1 eV versus NHE and the charge carrier density 2.6×10^{20} carriers cm^{-3}. Transient absorption spectroscopy revealed a transient species decaying on the microsecond timescale characterized by a broad band spanning 300–750 nm. This transient was attributed to the charge-separated state. These results are promising for the development of novel photocatalytic materials based on framework metal phosphate.

Introduction

Photocatalysis is fast gaining importance because, in addition to the degradation of pollutants in the gas or liquid phase, it could also be an alternative for solar light conversion.[1–5] Owing to the shortage of fossil fuels, considerable effort is being focused on the development of renewable energies. Sunlight reaching the Earth's surface is one of the primary energy resources and could provide enough energy to cover future energy demand.[6–9] However, due to the low power density of solar light, the diurnal cycle and the dependence of weather, solar light as a renewable energy has to be combined with energy vectors that accumulate and concentrate the solar energy. One possible strategy is the generation of hydrogen from water or the production of other solar fuels based on solar light photocatalysis.[7,10–16]

In photocatalysis, the energy of light is converted by a solid into chemical energy.[17–22] In typical photocatalysts, the absorption of a photon leads to the generation of a charge-separated state. The most widely used photocatalyst, also for the production of hydrogen and solar fuels, is titanium dioxide.[17,19,21] This solid presents several advantages under UV light irradiation, including availability, lack of toxicity and high photocatalytic efficiency; however, TiO_2 presents severe limitations that have proven difficult to overcome.

The most important limitations of TiO_2 as photocatalyst are its wide band gap and the large degree of charge recombination. For these reasons, the performance of TiO_2 as photocatalyst under sunlight illumination is far from optimal and there is continuing interest in developing new photocatalysts. Also of relevance for the present work is the discovery of the photoelectrochemical activity of α-Fe_2O_3 powders for the generation of hydrogen from water.[23–28] Two of the main advantages of iron oxide are its lack of toxicity and large abundance. However, the low reduction potential of its conduction band electrons (–0.4 eV vs. NHE[29]) is a major drawback in photocatalysis, making the reduction of water to H_2 thermodynamically uphill. To overcome this barrier it is necessary to submit the α-Fe_2O_3 photoanode to a bias potential of about 1 V. In addition, α-Fe_2O_3 tends to undergo photocorrosion, leading to the dissolution of Fe^{3+} during the photocatalytic reaction. In this context it is important to evaluate other water-insoluble iron compounds that could act as photocatalysts.

Considering the interest in developing new photocatalysts, we report herein the photocatalytic activity of open-framework iron hydroxyl phosphate (FeP) for H_2 generation from CH_3OH/H_2O that is comparable to that of commercial TiO_2 P25 under simulated sunlight irradiation.

[a] Instituto Universitario de Tecnologia Quimica, Universidad Politécnica de Valencia,
Avenida de los Naranjos S/N, 46022 Valencia, Spain
E-mail: hgarcia@qim.upv.es
www.upv.es/herme

Supporting information for this article is available on the WWW under http://dx.doi.org/10.1002/ejic.201500629.

Open-framework phosphates are materials that in contrast to bulk phosphates only contain metal–O–P linkages leaving interstitial channels in which a protonated amine remains entrapped compensating the net negative charge of the lattice. As will be shown below, compared with TiO_2, FeP has the additional advantage of being easy to dope. We have found that the photocatalytic activity of FeP depends on the nature and percentage of the dopant. Its semiconductor properties were characterized by measuring the conduction band potential, band gap, density of charge carriers and, by transient absorption spectroscopy, charge-separated state.

Because phosphates can be prepared by hydrothermal crystallization in the presence of a large variety of metals in a range of concentrations resulting in doping, our findings may lead to new openings in the search for novel efficient photocatalysts. There is only one report in the literature on the use of $Fe(OH)PO_4$ as a photocatalyst for the degradation of Methylene Blue under visible-light irradiation,[30] but until now the photocatalytic activity for hydrogen generation remains unexplored. In addition, we also show the ability of metal doping to increase the efficiency of FeP as a photocatalyst.

Results and Discussion

In the initial part of our study, open-framework FeP was synthesized by hydrothermal crystallization of an aqueous solution of iron chloride, ethylenediamine as base and templating agent, and phosphoric acid as phosphate source at 150 °C following a reported procedure.[31] In addition to FeP containing a single metal, a wide range of FePs containing 0.25–5 wt.-% Cr, Mn or Co were also synthesized. The possibility of doping FeP has already been considered in the literature. Specifically, we prepared three families of materials based on FeP containing three different dopant elements; their main analytical and characterization data are summarized in Table 1.

The samples based on FeP exhibit X-ray diffraction patterns typical of those previously reported for one-dimensional, open-framework iron hydroxyl phosphate.[31] Figure 1 shows selected XRD patterns for some of the FeP samples as well as the structure of these materials as reported in the literature.[31,32]

Noteworthy is the fact that the crystallinity of FeP is maintained with some minor variations in the peak intensity in the presence of the dopant elements. The almost coincident cationic radii of Fe, Cr, Mn and Co, as well as their similar charge densities, allows their incorporation in a few percent into the FeP structure without noticeable variation of the XRD pattern. The crystal structure of FeP consists of chains of octahedra with one Fe^{3+} ion at the centre and two vertices in *trans* positions sharing OH groups. Phosphate anions define tetrahedra around P^{5+} ions connected by two oxygen atoms to two different octahedra with one O atom and an OH group at the other two vertices. Ethylenediamine, present in the diprotonated form, occupies the interstitial space between the chains of octahedra, forming interactions with the octahedra through strong electrostatic forces and hydrogen bonds.

Table 1. Code, composition and photocatalytic data for the FeP samples under study.

Code[a]	Metal [wt.-%] dopant	Fe	H_2 production[b] [μmol]	H_2 producton[b] [μmol g_{Fe}^{-1}]
FeP [c]		100	0.36 ± 0.05	15 ± 2
(0.25Cr) FeP	Cr:0.28	99.7	0.54 ± 0.07	22 ± 4
(0.5Cr) FeP[c]	Cr:0.48	99.5	0.83 ± 0.06	34 ± 5
(1Cr)FeP [c]	Cr:90	99.1	0.87 ± 0.06	36 ± 5
(2Cr) FeP	Cr:2.30	97.7	0.64	26.
(5Cr) FeP	Cr:4.0	96.0	0.63	26
(0.25Mn) FeP	Mn:0.20	99.8	0.51	21
(0.5Mn) FeP	Mn:0.35	99.65	0.46	19
(1Mn) FeP	Mn:1.0	99.0	0.42	17
(2Mn) FeP	Mn:1.20	98.8	0.37	15
(5Mn) FeP	Mn:3.3	96.7	0.36	15
(0.25Co) FeP	Co:0.13	99.87	0.53	22
(0.5Co) FeP	Co:0.27	99.73	0.54	22
(1Co) FeP	Co:0.42	99.58	0.6	25
(2Co) FeP	Co:0.80	99.2	0.55	23
(5Co)FeP	Co:2.1	97.9	0.38	16

[a] The empirical formula of the FeP photocatalyst is $(C_2N_2H_{10})$-$Fe_{(1-x)}M_x(HPO_4)_2(OH)$ H_2O with M = Cr, Mn or Co. [b] H_2 production after 6 h irradiation with a solar simulator. [c] Average of four independent measurements.

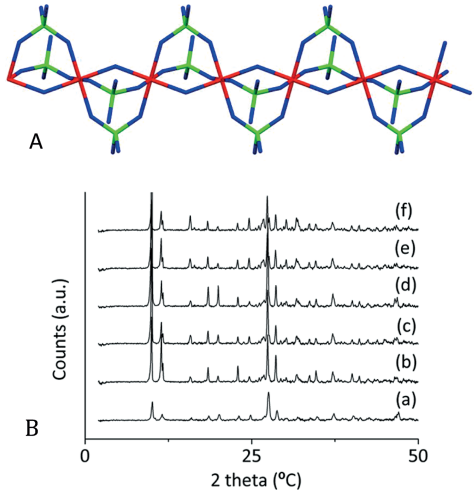

Figure 1. (A) Building blocks of FeP viewed along the *b* axis. Red atoms correspond to iron, green to phosphorus and blue to oxygen. Hydrogen atoms, ethylenediamine and water molecules have been omitted for clarity. The model of the Fe–O–P(O)–O chains was obtained by using the Mercury program for the structure file.[31,32] (B) XRD patterns of metal-doped samples: (a) FeP, (b) (0.25 Cr) FeP, (c) (0.5 Cr) FeP, (d) (1 Cr) FeP, (e) (2 Cr) FeP and (f) (5 Cr) FeP. For the XRD patterns of the other samples, see the Supporting Information.

The morphologies of the FeP particles were determined by microscopy; the large size of some of the particles in this case allowed the use of optical microscopy. Figure 2 shows representative images of FeP; the material is formed from a broad distribution of crystals with a long aspect ratio. Some of the particles are as long as 100 μm, and others have a length of about 1 μm. These sub-millimetric crystals are

formed by the aggregation of much smaller sheets. Scanning electron microscopy revealed in better detail that the crystals are in reality aggregates of a multitude of flakes with a thickness of about 0.5 μm and a length typically greater than 20 μm (see also Figure 2, bottom).

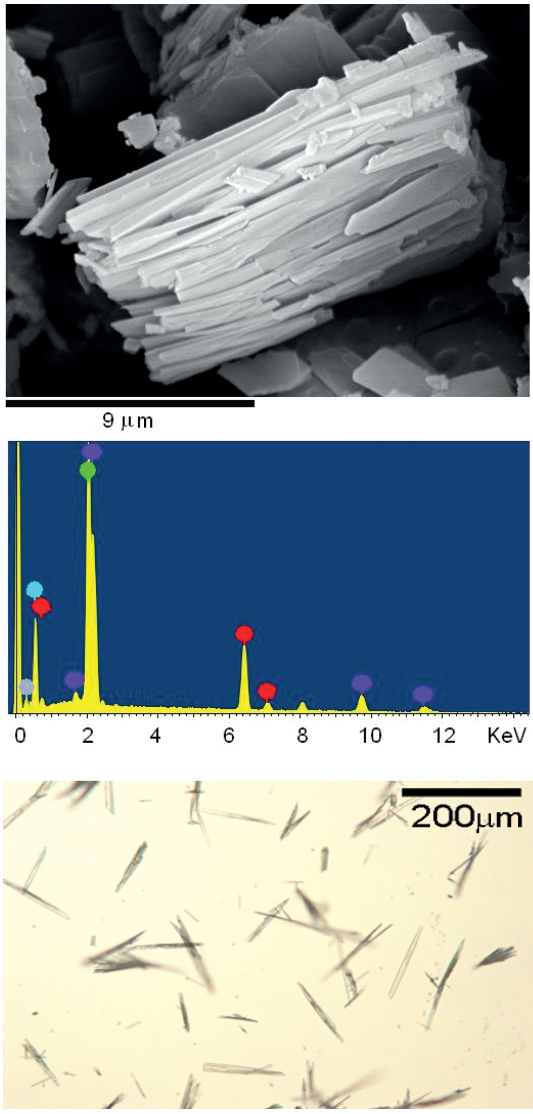

Figure 2. Top: SEM image recorded for FeP. Middle: EDS elemental analyses of the crystal showing the presence of Fe and P (purple: Au; red: Fe; green: P; blue: O; grey: C). Bottom: Optical microscopy image at a different magnification showing the large crystals present in FeP.

Of relevance with regard to the photocatalytic activity of the FeP samples are the optical absorption spectra, which are very similar regardless of the nature of the dopant and its percentage in the range 0.25–5 wt.-% (Figure 3). All the samples exhibit two minor absorption maxima at 380 and 420 nm, which can be attributed to the d–d transition of Fe^{3+} ions. These peaks are accompanied by an intense absorption band at 280 nm, attributable to the ligand-to-metal O–Fe charge-transfer band.

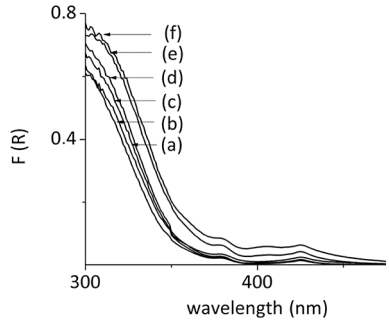

Figure 3. Diffuse reflectance UV/Vis absorption spectra (plotted as the Kubelka–Munk function of the remittance, *R*) of metal-doped FeP: (a) FeP, (b) (0.25 Cr) FeP, (c) (0.5 Cr) FeP, (d) (1 Cr) FeP, (e) (2 Cr) FeP and (f) (5 Cr) FeP. For the UV/Vis spectra of the other doped FeP samples, see the Supporting Information.

All the FeP samples under study exhibited photocatalytic activity for H_2 generation under simulated solar light irradiation in H_2O/CH_3OH. No hydrogen evolution was observed for FeP in the absence of CH_3OH under the same conditions. Figure 4 shows the evolution of hydrogen for the undoped FeP sample. The sample exhibits an induction period of about 1 h in which little H_2 is produced.

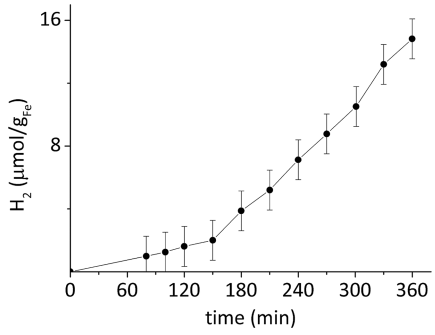

Figure 4. Photocatalytic hydrogen production from water/methanol mixtures using FeP as photocatalyst under simulated sunlight irradiation. Vertical bars represent the relative error of the measurements. Reaction conditions: water/methanol (1:1, 25 mL), 1 g L^{-1} catalyst concentration.

This induction period could be related to possible modifications of the oxidation state of Fe^{3+} in FeP or to the adsorption of hydrogen on the solid before being detectable in the gas phase. However, the H_2 adsorption on FeP at room temperature measured independently was negligible. It is important to mention that H_2 is produced in the presence of a photocatalyst that does not contain any noble metal such as Pt as co-catalyst.

Irradiation with monochromatic light at 300 (0.09 mW m^{-2}) and 420 nm (5.8 mW m^{-2}) led to the generation of 0.54 and 0.58 μmol of hydrogen in 6 h. The fact that a higher light power at 420 nm results in a similar generation of hydrogen as achieved with irradiation at 300 nm is probably a reflection of the much higher absorption at 300 nm of FeP (Figure 3).

It should be commented that 2.4 μmol of H_2 were produced with P25 TiO_2 under the same conditions as those shown in Figure 4 at 6 h (96 μmol g^{-1}), which is about six-

fold higher than that measured for FeP. It should, however, be noted that this comparison is based on the same photocatalyst weight. More accurate comparisons should be based on quantum efficiencies that reflect intrinsic photocatalytic activity.

Concerning stability, the chemical analysis of the solution after 6 h of irradiation and removal of the solid catalyst showed an iron content below 10 ppb, which indicates that the possible amount of Fe^{3+} leached from the photocatalyst has to be below 0.005% of the initial Fe^{3+} content.

This analytical data showing negligible Fe^{3+} leaching together with the lack of apparent change in the XRD patterns of the FeP samples after prolonged irradiation indicate the stability of FeP as photocatalyst. The results shown in Figure 4 have to be considered in the context of the lack of hydrogen production in the absence of a bias potential of α-Fe_2O_3[26] and the low photostability of this oxide resulting in leaching Fe^{3+} into the solution and dissolution of the solid.[28]

The influence of doping on the photocatalytic activity for hydrogen generation is presented in Figure 5. As can be seen, for the three sets of samples the activity towards hydrogen production is optimal when the dopant loading is between 0.1 and 1 wt.-%, lower or higher loadings resulting in a decrease in the photocatalytic activity. Also, the nature of the dopant element has an influence, chromium showing the highest photocatalytic activity. According to the data shown in Figure 5, the amount of hydrogen can be increased by a factor 2.5 by incorporating chromium in a percentage of about 1%.

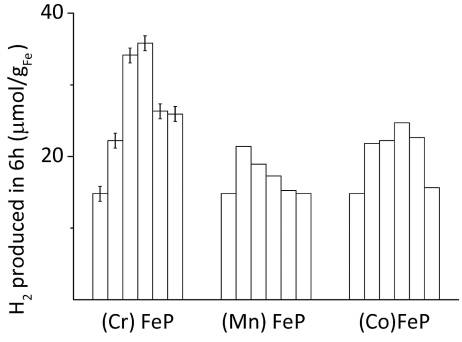

Figure 5. Hydrogen production from water/methanol at 6 h irradiation using doped FeP as photocatalysts under simulated sunlight irradiation. Reaction conditions: water/methanol mixtures (1:1, 25 mL), catalyst concentration 1 g L^{-1}. Concentration of dopant element increases for each dopant from left to right: 0, 0.25, 0.5, 1, 2 and 5%.

In analogy with TiO_2, we propose that in the present case metal doping should operate by increasing the efficiency of charge separation. It is known that upon light absorption and the generation of electrons in the conduction band and holes in the valence band, ultra-fast charge recombination is the main deactivation pathway, limiting the efficiency of the photocatalytic reactions.[17] Doping can introduce into the interband gap space additional states that can act as traps of electrons or holes, promoting charge separation and/or increasing the lifetime of the charge-separated state. Our proposal to explain the influence of doping and the more efficient hydrogen generation by doped semiconductors is illustrated in Scheme 1. The fact that there is an optimal doping level suggests that the positive effect of the dopant increasing the efficiency of charge separation by providing interband gap trapping sites is offset by an increase in charge recombination efficiency caused at higher dopant concentrations.[21]

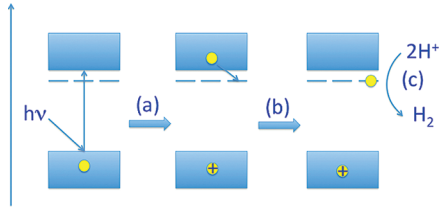

Scheme 1. Possible explanation of the influence of metal doping in FeP on charge separation and hydrogen production. The top and bottom blue rectangles correspond to CB and VB, respectively. The dashed line below the CB corresponds to the interband gap state introduced by the dopant element. (a) Charge separation; (b) migration of conduction band electrons to the dopant level; (c) H^+ reduction.

All the above data refer to irradiation with simulated solar light containing about 4% of the energy in the UV region and about 42% of the energy in the visible range. Owing to the lack of photocatalytic activity of titanium oxide under irradiation with visible light, there is continuing interest in the development of visible-light photocatalysts.

In the present case, and considering that according to the absorption spectra the samples absorb light in the visible region, we were interested in determining whether the doped FeP samples exhibit some photocatalytic activity in visible light. To address this issue we performed a set of photocatalytic tests using a 450 nm LED emitting light of wavelength above 420 nm (50 mW cm^{-2} at a distance of 3 cm, see the emission spectra in the Supporting Information). All the samples exhibited under these conditions weak but measurable photocatalytic activity. The hydrogen generation in the presence of Cr-doped FeP under visible light is presented in Figure 6. The results obtained indicate

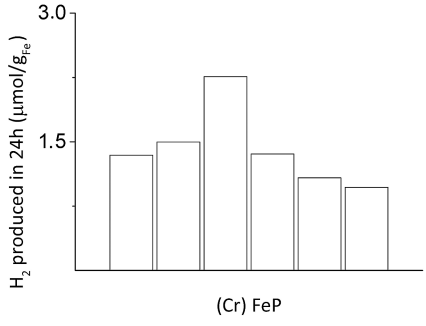

Figure 6. Hydrogen production from water/methanol mixtures using (Cr)FeP as photocatalysts and a visible-light LED as the irradiation source. Reaction conditions: water/methanol (1:1, 25 mL), 1 g L^{-1} catalyst concentration, 24 h. Concentration of dopant element increases from left to right: 0, 0.25, 0.5, 1, 2 and 5%.

that under simulated sunlight a considerable proportion, about 66%, of the photocatalytic activity is due to the UV light even though this wavelength range corresponds to a minor percentage of the total solar energy.

The conduction band flat potential for FeP was estimated by measuring the photocurrent against the bias potential, determining the value that changes the photocurrent from positive to negative. These measurements gave a flat band potential of 0.1 eV. In addition, impedance spectroscopy of thin FeP films on transparent conductive electrodes (see Figures S4 and S5 in the Supporting Information) allowed us to estimate values of 0.1 eV and 2.6×10^{20} carriers cm^{-3} for the flat band potential and the density of charge carriers, respectively.

The charge-separation state and its quenching behaviour as well as the influence of metal doping were monitored by nanosecond transient absorption spectroscopy using a 266 nm laser as the excitation source. In these experiments FeP samples were suspended in acetonitrile by sonication. After removal of the solid residues by decantation, the persistent FeP colloidal solutions were submitted to nanosecond laser flash excitation. Regardless of the presence of dopant elements, all the transient spectra were characterized in the microsecond timescale by a continuous absorption spanning the whole wavelength range. As an example, Figure 7 shows the transient spectra for FeP observed at 1.9, 5.8, and 10.8 μs after the laser flash. The time profiles of the signal at different wavelengths are coincident, which suggests that it corresponds to the same transient.

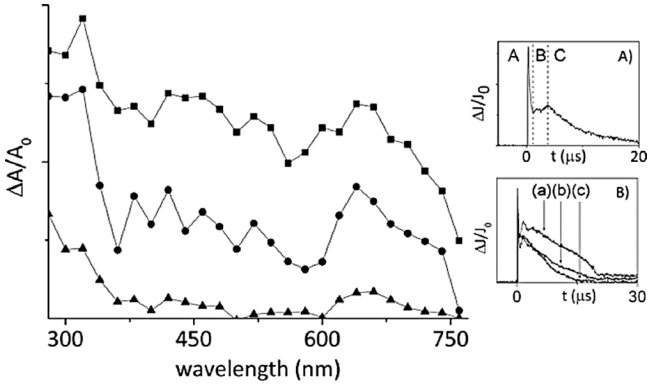

Figure 7. Transient absorption spectra recorded for N_2-purged FeP suspended in acetonitrile (OD = 0.3 at 355 nm) at 1.9 (■), 5.8 (●) and 10.78 μs (▲) after 355 nm laser excitation. Inset A: Time profile of the transient spectrum monitored at 400 nm. The profile shows three kinetic regimes that have been labelled A, B and C. Inset B: Time profile of the signal at 420 nm for the FeP suspension in acetonitrile (OD = 0.31 at 355 nm) after 355 nm laser excitation (the plots a, b and c correspond to the temporal profiles after N_2 and O_2 purging or in presence of methanol, respectively).

The time profile shows three kinetic regimes (see Figure 7). The first one is a fast decay, taking place in less than 0.15 μs and corresponding to more than 60% of the top $\Delta J/J_o$. This fast decay is followed by a growth from 0.15 to about 2.0 μs, the $\Delta J/J_o$ signal increasing by about 10%. The third kinetic regime corresponds to the final decay of the signal from 2.5 to 20 μs. As we will see below, quenching experiments revealed that this transient corresponds to the fraction of the charge-separated state of FeP materials decaying on the microsecond timescale. In accord with this, the three kinetic steps could correspond to a fast charge recombination (regime A) followed by charge migration and relocation into traps (regime B), and a final recombination of the free charge carriers (regime C).

No influence of the dopant elements either on the spectra or on time profiles was observed. However, we noted that the intensity of the signal immediately after the laser pulse is dependent on the nature of the dopant. This observation suggests that the dopant element may disfavour the ultrafast charge recombination of charge carriers on the submicrosecond timescale rather than the relocation or recombination kinetics on longer timescales because the last two factors would have led to changes in the transient spectra or the transient signals. According to the proposal presented in Scheme 1, steps a and b should occur on timescales shorter than microseconds and the trapping will be manifest on the microsecond timescale as an increase in the intensity of the initial density of the charge separation.

The time profile of the signal is sensitive to the presence of quenchers (Figure 7). In the present study we used oxygen as conduction-band electron quencher and methanol as valence-band hole quencher. In the case of FeP, the presence of oxygen increases the intensity of the signal corresponding to regimes A and C (Figure 7) and methanol increases more significantly the signal in region C (Figure 7). This effect of the quencher increasing the intensity of the signal without significantly affecting the kinetics of the decay can be interpreted by considering geminate charge recombination of electron and holes as the main decay pathway of the signal. If one quencher is present partially removing one of the charge carriers, then the transient signal can increase due to the detection of the complementary charge that has not collapsed by recombination and therefore reaches the nanosecond timescale in larger concentrations. The influence of oxygen and methanol on the time profile of the signal is in agreement with the assignment of the transient spectra to the combined absorption of electrons and holes. And the transient detected on the microsecond timescale being a fraction of the total charge separation events, specifically, the population of charge-separated states that disappear on the sub-microsecond timescale. As an example, Figure 7 shows the time profiles of the signal monitored for FeP under argon- or oxygen-purging or in the presence of methanol. Interestingly, the time profiles for doped FeP follow the same general trend observed for undoped FeP. The most salient feature of O_2 and CH_3OH quenching in the presence of doped FeP, particularly in regime C, is the considerably smaller effect than that presented in Figure 7 for FeP. Regardless of the initial value of $\Delta J/J_o$, at short delay times the signal for doped FeP is clearly influenced by the presence of the quenchers, but the signal decay at longer times is almost insensitive to the presence of O_2 or CH_3OH. This could be due to the trapping of charge carriers at certain sites.

Conclusions

The results presented herein illustrate the potential of widely available FeP as photocatalysts for hydrogen production, combining the advantages of photostability, a higher reduction potential of the conduction band electrons than α-Fe_2O_3 and easy doping during the synthesis of the materials. Our results show that doping with metal elements can increase the photocatalytic activity of FeP by a factor of 2.5.

The behaviour of FeP as a semiconductor has been supported by photocurrent measurements and impedance spectroscopy, which have allowed the positions of the conduction and valence bands to be established and an estimation of the density of carriers. The charge-separated state was detected by transient absorption spectroscopy. The transient absorption spectrum shows a continuous absorption band spanning the whole wavelength range exhibiting three kinetic regimes and decaying completely in 20 μs. Assignment of the transient spectrum was based on the behaviour of the signal in the presence of oxygen and methanol, which are typical electron and hole quenchers, respectively. Dopant elements influence the intensity of the transient signal, which is more intense in the presence of dopants. In addition, the interaction of the dopant elements with quenchers renders these materials less sensitive to quenchers.

Thus, the present findings may open the way to the further development of a novel family of semiconductors with promising applications as photocatalysts based on the affordable elements iron and phosphorus.

Experimental Section

Material Preparation: Open-framework iron hydroxyl phosphate (FeP) was prepared as reported by Song and co-workers.[31,32] In brief, an aqueous solution of ferric chloride, phosphoric acid and ethylenediamine ($FeCl_3$ 0.005 mol/H_3PO_4 0.04 mol/$NH_2CH_2CH_2NH_2$ 2.5 mL/H_2O 35 mL) was placed in a 200 mL Teflon-lined autoclave using a filling factor of 75%. The autoclave was heated at 150 °C for 2.5 h and after this time the reaction mixture was cooled to room temperature using an ice bath. The resulting precipitate was filtered, washed and dried in vacuo at room temperature. The doped materials were prepared following the same synthetic protocol using a mixture of ferric chloride and chromium, manganese, or cobalt chloride as dopant in proportions ranging from 0.25–5 wt.-%.

Photocatalytic Tests for Hydrogen Production: A suspension of the catalyst (25 mL, 1 gL^{-1}) was sonicated for 10 min and placed in a closed reactor with an irradiation window of 12.56 cm^2 and temperature and pressure controllers. The reactor was placed in a thermostatic bath with the temperature set to 25 °C. The suspension was purged with an argon flow of 2 psi for 15 min prior to irradiation. The photoreaction was performed from the top of the photoreactor by using a visible-light LED or a solar simulator (Thermo Oriel 1000 W) with an irradiation spot of 100 cm^2, placed at a distance of 10 cm. The light of the solar simulator was filtered through an Air Mass 1.5 filter and consists approximately 4% of UV light. The amount of hydrogen collected in the headspace of the reactor was analysed by injecting 100 μL of the gas into a gas chromatograph equipped with a MOLSieve column and a TC detector with argon as thee carrier gas.

Photocurrent Measurements and Determination of the Flat Band Potential of the Conduction Band: For photocurrent measurements, thin films of FeP were deposited onto an FTO electrode ("Solaronix" 0.8 × 10 cm^2). Deposition was performed by spreading a paste containing the semiconductor on the FTO surface by using the doctor blade procedure. The surface of the FTO was defined by adhesive tape. The paste containing the semiconductor was prepared in advance to the deposition of the film onto the electrode by dispersing FeP (100 mg), acetone (1 mL) and α-terpineol (1 mL). The suspension was stirred for 24 h to achieve a homogeneous dispersion. Then the acetone and α-terpineol were allowed to evaporate at room temperature to obtain the final dense semiconducting paste. After deposition of the paste, the adhesive tape was removed and the semiconductor film on FTO was heated at 80 °C for 24 h to increase the mechanical adherence to the layer. Photocurrent measurements were carried out by using a 150 W Xenon arc lamp as light source and a PTI model 101 monochromator. Electrical currents were measured with an Amel 7050 potentiostat connected electrically to the FTO electrode with a platinum wire as counter electrode. The experiments were conducted inside a quartz cuvette (20 mL) containing an aqueous 0.1 M KCl solution as electrolyte. The system was purged with nitrogen for at least 15 min before measurement. Flat conduction band potentials were determined by measuring the photocurrent by applying an increasing bias from 0.3 to –0.3 V s. (vs. Ag/AgCl) every 0.1 V (seven points). The photocurrent onset was detected at 365 nm and a scan rate of 2 min was used, namely 1 min without irradiation followed by 1 min illumination of the cell.

The number of charge carriers was determined by using the same system connected to a frequency response analyser. The measurements were taken from 0.5 to –0.1 V every 0.1 V (seven points). At each voltage the system was scanned in the frequency range from 105 from 0.1 Hz.

Transient Absorption Spectroscopy: Suspensions of FeP or doped FeP in acetonitrile were prepared by sonicating the powder for 10 min at 150 W. The amount of solid was set to obtain an optical density at 266 of 0.35 units. The suspensions were persistent during the time needed for the transient absorption spectra measurements (about 3 h) without deposition of any solid. The suspensions in acetonitrile (3 mL) were placed in Suprasil quartz cuvettes of 1 × 1 cm^2 capped with septa. The suspensions were purged with argon or oxygen (for quenching experiments) for at least 15 min before the measurements. For the quenching experiments with methanol, argon was bubbled through a bottle of methanol and passed through the FeP suspensions for at least 50 min before measurement. Transient measurements were carried out by using the fourth harmonic (266 nm, 20 mJ $pulse^{-1}$) of a Nd:YAG laser (7 ns fwhp) as the excitation source. The transient signal was recorded in transmission mode using a 150 W xenon lamp as the monitoring beam through fibre optics to collect the transmitted light. The signal from the monochromator/photomultiplier detection system was captured by a Tektronix 2440 digitizer and transferred to a PC computer that controlled the experiment and provided suitable processing and data storage capabilities.

Acknowledgments

Financial support by the Spanish Ministry of Economy and Competitiveness (MEC) (Severo Ochoa and CTQ20212-32315) and the Generalidad Valenciana (Prometeo 2012/014) is gratefully acknowl-

edged. M. S. thanks the Spanish Consejo Superior de Investigaciones Científicas (CSIC) and Technical University of Valencia for a postgraduate scholarship.

[1] Y. Amao, *ChemCatChem* **2011**, *3*, 458.
[2] G. Centi, S. Perathoner, *ChemSusChem* **2010**, *3*, 195.
[3] D. Gust, T. A. Moore, A. L. Moore, *Acc. Chem. Res.* **2009**, *42*, 1890.
[4] L. Hammarström, S. Hammes-Schiffer, *Acc. Chem. Res.* **2009**, *42*, 1859.
[5] N. Serpone, D. Lawless, R. Terzian, *Solar Energy* **1992**, *49*, 221.
[6] D. Abbott, *Proc. IEEE* **2010**, *98*, 42.
[7] S. Dunn, *Int. J. Hydrogen Energy* **2002**, *27*, 235.
[8] P. V. Kamat, *J. Phys. Chem. C* **2007**, *111*, 2834.
[9] N. S. Lewis, D. G. Nocera, *Proc. Natl. Acad. Sci. USA* **2006**, *103*, 15729.
[10] A. J. Bard, M. A. Fox, *Acc. Chem. Res.* **1995**, *28*, 141.
[11] S. Bensaid, G. Centi, E. Garrone, S. Perathoner, G. Saracco, *ChemSusChem* **2012**, *5*, 500.
[12] X. Chen, S. Shen, L. Guo, S. S. Mao, *Chem. Rev.* **2010**, *110*, 6503.
[13] G. W. Crabtree, M. S. Dresselhaus, M. V. Buchanan, *Phys. Today* **2004**, *57*, 39.
[14] M. Gratzel, *Acc. Chem. Res.* **1981**, *14*, 376.
[15] M. Ni, M. K. H. Leung, D. Y. C. Leung, K. Sumathy, *Renewable Sustainable Energy Rev.* **2007**, *11*, 401.
[16] J. Nowotny, C. C. Sorrell, L. R. Sheppard, T. Bak, *Int. J. Hydrogen Energy* **2005**, *30*, 521.
[17] D. W. Bahnemann, *Res. Chem. Intermed.* **2000**, *26*, 207.
[18] M. A. Fox, M. T. Dulay, *Chem. Rev.* **1993**, *93*, 341.
[19] A. Fujishima, X. Zhang, D. A. Tryk, *Surf. Sci. Rep.* **2008**, *63*, 515.
[20] J. M. Herrmann, *Catal. Today* **1999**, *53*, 115.
[21] A. L. Linsebigler, G. Q. Lu, J. T. Yates, *Chem. Rev.* **1995**, *95*, 735.
[22] A. Mills, S. LeHunte, *J. Photochem. Photobiol. A: Chem.* **1997**, *108*, 1.
[23] N. Beermann, L. Vayssieres, S. E. Lindquist, A. Hagfeldt, *J. Electrochem. Soc.* **2000**, *147*, 2456.
[24] U. Bjorksten, J. Moser, M. Grätzel, *Chem. Mater.* **1994**, *6*, 858.
[25] Y.-S. Hu, A. Kleiman-Shwarshtein, A. J. Forman, D. Hazen, J.-N. Park, E. W. McFarland, *Chem. Mater.* **2008**, *20*, 3803.
[26] A. Kay, I. Cesar, M. Graetzel, *J. Am. Chem. Soc.* **2006**, *128*, 15714.
[27] K. Sivula, F. Le Formal, M. Graetzel, *ChemSusChem* **2011**, *4*, 432.
[28] K. Sivula, R. Zboril, F. Le Formal, R. Robert, A. Weidenkaff, J. Tucek, J. Frydrych, M. Graetzel, *J. Am. Chem. Soc.* **2010**, *132*, 7436.
[29] M. Gratzel, *Nature* **2001**, *414*, 338.
[30] X. J. Wang, H. Pang, S. Zhao, W. Shao, B. Yan, X. Li, S. Li, J. Chen, W. Du, *ChemPhysChem* **2013**, *14*, 2518.
[31] Y. Song, P. Y. Zavalij, N. A. Chernova, M. Suzuki, M. S. Whittingham, *J. Solid State Chem.* **2003**, *175*, 63.
[32] Y. Song, P. Y. Zavalij, N. A. Chernova, M. S. Whittingham, *Chem. Mater.* **2005**, *17*, 1139.

Received: June 17, 2015
Published Online: August 11, 2015

